Meteorology of the Waldo Canyon Fire

Richard H. Johnson,[+] * Russ S. Schumacher,[+] James H. Ruppert, Jr.,[+] and Daniel T. Lindsey[#]

[+] *Colorado State University, Fort Collins, Colorado*

[#] *NOAA Center for Satellite Applications and Research, CIRA/CSU, Fort Collins, Colorado*

[*] *Corresponding author address:* Richard H. Johnson, Department of Atmospheric Science, Colorado State University, Fort Collins CO 80523.

E-mail: johnson@atmos.colostate.edu

ABSTRACT

The meteorological conditions associated with the catastrophic Waldo Canyon Fire of June 2012 have been investigated. The fire destroyed 347 homes in Colorado Springs and resulted in insurance losses of nearly $0.5B, making it the most economically destructive fire in Colorado's history. On the afternoon of the 26th, the Waldo Fire grew explosively and rapidly advanced eastward into a heavily populated area on the west side of Colorado Springs.

Unprecedented dry and hot conditions prevailed over the Intermountain West prior to the Waldo Fire, along with a persistent upper-level ridge. On June 26, a narrow tongue of moist air aloft originating over the Southwest shifted from Utah into Colorado. Along with dry conditions at lower levels, the stage was set for high-based thunderstorms and microbursts to develop over the region. Convective cells first formed at midday over the San Juan Mountains of southwestern Colorado. The cells later consolidated into a thunderstorm complex that produced an organized convective outflow with strong, gusty winds at the surface. The leading gust front associated with the outflow moved past the Waldo Fire at the hottest time of the day with wind gusts as high as 26 m s^{-1}. The blowup of the Waldo Fire and its rapid advance were timed with the passage of this strong gust front. A numerical simulation, initiated one day earlier, produced mesoscale features closely resembling those observed, including the gust front passage at the fire, indicating some predictability of the triggering of the fire blowup a day in advance.

1. Introduction

The fire season of 2012 was one of the most devastating on record for the Intermountain West. Extremely hot, dry conditions led to numerous wildland fires throughout the region, many of which occurred in Colorado. Among these, the Waldo Canyon Fire near Colorado Springs has proven to be the most economically destructive in Colorado's history. It resulted in two fatalities, destroyed 347 homes,[1] consumed over 18,000 acres of forest, and led to insurance claims totaling $454M (http://www.denverpost.com). While the stage for the Waldo Canyon Fire was set by a prolonged drought and excessive heat over the region, short-term meteorological events played a key role in the fire's explosive growth on June 26 at the urban-forest interface on the west side of Colorado Springs.

On the afternoon of June 26, the Waldo Canyon Fire surged eastward out of the foothills into housing developments on the west side of Colorado Springs. In a matter of hours, hundreds of homes were enveloped by the fire, many by embers blown out ahead by strong westerly winds aloft. The fire had been slowly growing for several preceding days, but its rapid intensification and expansion during the afternoon of the 26th was dramatic (Fig. 1). The area of the fire nearly tripled in size in one day (Fig. 2). This event had the characteristics of a "blowup" fire (Potter 2012a), defined by the Glossary of Wildland Fire Terminology as the 'sudden increase in fireline intensity or rate of spread of a fire ... often accompanied by violent convection and may have other characteristics of a fire storm.' The rapid intensification of the fire was accompanied by the development of pyrocumulus clouds (Fromm et al. 2010) in the late afternoon/early evening (Fig. 1).

The explosive growth of the Waldo Canyon Fire within a residential area necessitated an immediate response to avoid loss of life. As a result of the swift action of emergency management teams and timely communication via local and social media, over 30,000 people were safely evacuated from affected neighborhoods just prior to the arrival of the fire front

[1] In terms of homes lost, the Waldo Canyon Fire has now been exceeded by the mid-June 2013 Black Forest Fire northeast of Colorado Springs, where 511 homes were destroyed.

(Meister 2013; Stark 2013). The devastation to homes was sudden and nearly complete in many neighborhoods, so the timely response to the rapidly advancing fire was vital.

Mesoscale and radar analyses show that the blowup of the Waldo Canyon Fire was timed with the arrival a thunderstorm gust front that swept through the Colorado Springs area during the afternoon of June 26. The convective outflow, which had the characteristics of a macroburst (Fujita 1985), grew out of a thunderstorm complex that had its first origins over the mountains of southwest Colorado. This paper documents the synoptic-scale conditions that contributed to the formation of macroburst-type thunderstorms on that day, the development of incipient convection in southwestern Colorado, and the progression of the associated gust front through the Waldo Canyon Fire area. The passage of the gust front led to an abrupt change in the fire characteristics. In addition to the observational study, a numerical modeling investigation has been carried out where it is shown that macroburst-producing storms contributing to the blowup of the fire on June 26 were predictable at least a day in advance.

2. Background

Anomalously warm and dry conditions prevailed throughout the Intermountain West in the months prior to the outbreak of the spring and summer wildland fires of 2012. The January-June 2012 period was the second driest and second warmest in Colorado in 118 years of record, while many other states in the region had similar near-record conditions (Fig. 3). Below-average late-winter snowpacks were compounded by a very dry and warm spring such that spring and early summer runoff over most of the region was well below average, and in many Colorado river basins worse than 2002 or other benchmark dry years for the region (1977, 1992) (source: http://wwa.colorado.edu). This situation led to very dry fuel conditions throughout the state. By a substantial margin, 2012 broke the previously held March-April-May mean temperature record for the United States that occurred in 1910,

the year of "The Big Burn" forest fire in northeast Washington, northern Idaho, and western Montana (Diaz and Swetnam 2013).

The Waldo Canyon Fire started along a trail area within the canyon early on June 23 (Fig. 2). As of this writing, the cause of the fire has not yet been determined. The burn area grew slowly over the next several days, but on the afternoon of June 26 the fire rapidly intensified and spread to the north and east (Fig. 2). The focus of this study is on the meteorological conditions accompanying the sudden blowup of the fire. Such rapid changes in wildland behavior, termed *extreme fire behavior* (Werth et al. 2011), are not uncommon. The prediction of and response to such changes are of critical importance for the protection of life and property.

General conditions conducive to wildland fires have been recently reviewed by Potter (2012a). Primary contributing factors are extreme heat, drought, and dry fuels. Such conditions were clearly present leading up to and during the Waldo Canyon event. In addition, unstable or near-neutral stratification in the lower troposphere accompanied by strong wind shear can promote wildland fire growth. In many fires, there is an interaction or coupling between the atmosphere and the fire itself to create "fire storms" containing distinct fire weather phenomena: intense fire plumes (Taylor et al. 1973; Kiefer et al. 2009), fire vortices and fronts (Clark et al. 1999), fire-generated downbursts (Goens and Andrews 1998), and even tornadogenesis (Cunningham and Reeder 2009). Downdrafts within fire storms can transport higher momentum down to the surface that serves to intensify and spread the fires. With sufficient moisture, either from the environment or from moisture released during combustion, fires can create pyrocumulus (Fromm et al. 2010; Lang et al. 2013), which in turn can result in rapid expansion of fires through associated storm circulations (Clark et al. 1996; Potter 2012b). The dramatic changes in the Waldo Canyon Fire during the afternoon on June 26 (Fig. 1) could have been a consequence of a number of these phenomena; however, the case will be made that it was the passage of a strong gust front through the area that led to the rapid eastward advance of the fire front. The impact of the gust front

was exacerbated by the fact that it occurred during the hottest part of the day when, apart from other effects, wildland fires typically intensify (e.g., Fromm et al. 2010). Compounding the situation, Denver tied and Colorado Springs set their all-time maximum temperature records on that same day (40.6°C or 105°F and 38.3°C or 101°F, respectively).

Previous instances of significant synoptic or mesoscale weather impacts on fire behavior have been reported. In July 1994, the passage of an unusually strong upper-level trough over the Rocky Mountain states caused a sudden shift and strengthening of the winds that trapped and took the lives of 14 firefighters working on the South Canyon Fire near Glenwood Springs, Colorado (Butler et al. 1998). Recently, Engel et al. (2012) investigated the impact of various synoptic-to-mesocale features on the evolution of the 7 February 2009 'Black Saturday' fires over the state of Victoria, Australia. They found that boundary layer horizontal convective rolls, unsteady gravity currents, and nocturnal bores modified the local environment leading to large spatial and temporal variability in the fire behavior. And most recently, the rapid spreading of the July 2013 Yarnell Fire in Arizona by a gust front claimed the lives of 19 firefighters. The need to anticipate and accurately forecast such meteorological events is of obvious importance for both firefighters and the preparation of timely warnings to the affected communities.

3. Data and modeling procedures

a. Data for synoptic-scale and mesoscale analyses

A map of the various sites that collected data used in subsequent mesoanalyses is shown in Fig. 4. A mix of surface observations have been utilized: National Weather Surface (NWS) ASOS (Automated Surface Observing System) from the National Oceanic and Atmospheric Administration (NOAA) National Climatic Data Center (NCDC; http://www.ncdc.noaa.gov/), Remote Automated Weather System (RAWS), and Snow Telemetry (SNOTEL) stations. Data from the latter two sources have been obtained from the University of Utah MesoWest

website (http://mesowest.utah.edu: Horel et al. 2002). Surface data from these networks are used to identify and track outflow boundaries from thunderstorms originating at midday over southwest Colorado. Surface mesoanalyses are complicated owing to the complex and mountainous terrain of the region, the irregular frequency and spacing of the surface observations, and the inconsistent data quality from the diverse platforms. Nevertheless, the ability to investigate mesoscale phenomena in the Intermountain West has been vastly improved over the past two decades by the advent of enhanced surface observations in support of fire weather operations, water resource management, and other applications (Myrick and Horel 2008; Steenburgh et al. 2009).

Sounding data were obtained from the University of Wyoming (http://weather.uwyo.edu/upperair/sounding.html). Data for synoptic-scale analyses were based on the Global Forecast System (GFS) archive at the NOAA National Operational Model Archive and Distribution System (NOMADS: http://nomads.ncdc.noaa.gov/).

b. Radar and satellite data

Level-II WSR-88D (Weather Surveillance Radar 88 Doppler) radar reflectivity and velocity data from Pueblo (PUX) and Denver (FTG), Colorado (Fig. 4), are utilized to track the progression of gust fronts across the Colorado Springs area. To produce a large-scale mosaic of the radar reflectivity field for a set of mesoanalyses, base-scan reflectivity data ($\sim$0.5°) were collected for a given time from PUX and FTG, and the data points nearest to their parent station were plotted. This procedure exploits the lowest reflectivity data possible from the two stations. The Gibson Ridge GR2Analyst software package is employed to create vertical cross sections of the radar reflectivity and radial velocity fields from the PUX WSR-88D data as well as 3-D displays (http://www.grlevelx.com/gr2analyst). Visible and infrared satellite data are obtained from GOES-15 and water vapor data from GOES-13.

c. Numerical simulations

The National Center for Atmospheric Research (NCAR) Weather Research and Forecasting Model (WRF) Advanced Research WRF (ARW: Skamarock et al. 2008) was run over a domain covering most of the central two-thirds of the United States (shown in Fig. 16, later) for 27 hours from 0000 UTC 26 June to 0300 UTC 27 June. The simulation used a 4-km horizontal grid spacing and 51 vertical levels on a stretched grid. Initial and lateral boundary conditions were from the 0.5 degree GFS model. The boundary conditions are based on GFS forecasts, so simulation could have been run in real time, i.e., it is technically a "reforecast." Physics packages include Morrison double-moment microphysics (Morrison et al. 2005), the Rapid Radiative Transfer Model (RRTMG: Iacono et al. 2008), and the Mellor-Yamada-Janjić (MYJ: Mellor and Yamada 1982; Janjić 2002) boundary layer scheme. Convection was treated explicitly, i.e., no cumulus parameterization was used.

4. Large-scale environmental conditions

a. Synoptic setting

The primary feature of the large-scale flow during this period was a strong, persistent ridge over the central United States and troughs on both the east and west coasts (Fig. 5). During the 24-h period from 0000 UTC on the 26th to 0000 UTC on the 27th (subtract 6 h to obtain local time), a shortwave trough moved across the Pacific Northwest in association with a slight flattening and eastward shift of the Central U.S. ridge (Figs. 5a,b). Over the same period, southerly to southwesterly flow increased over the southern Intermountain West as absolute vorticity maxima approached from the west. Maps of precipitable water over a three-day period starting at 0000 UTC 24 June (Fig. 6) reveal that this increased southerly-southwesterly flow aided the wrapping of an eastern-Pacific moisture tongue around a 700-hPa anticyclone, which led to increased moisture over the Colorado-Utah region by the

evening of June 26.

On the afternoon of 26 June, a surface low pressure area extended from eastern Colorado northward to eastern Montana (Fig. 7). Over Colorado, the feature took the form of a lee trough east of the Rocky Mountains, while the extension of the low over Montana was associated with the shortwave trough moving inland from the west coast (Fig. 5b). The lee trough along the Colorado Front Range led to moderate southwesterly low-level flow across the Waldo Canyon Fire area. The eastern-Pacific moisture tongue in precipitable water (Fig. 6d) is reflected at the surface as a region of high surface equivalent potential temperature (>360 K) over Arizona, which is being advected towards Colorado by southwesterly flow (Fig. 7).

Soundings in the late afternoon on the 26th from Denver and Grand Junction, Colorado, representing conditions across the state, are shown in Fig. 8. At both stations the temperature and moisture stratification have nearly ideal characteristics of a "microburst" sounding, as described by Wakimoto (1985). Nearly dry adiabatic and constant specific humidity profiles from near the surface to 500 hPa (an "inverted-V" pattern) are conducive to strong downdrafts if precipitation develops from clouds in the layer above. Downdraft convective available potential energy (DCAPE: Gilmore and Wicker 1998) in the DNR sounding was exceptionally large (1458 J kg^{-1}) compared to values reported in other high-wind situations (Kuchera and Parker 2006), further reinforcing the fact that the profile was conducive to strong downdrafts. As will be seen, precipitating clouds developed over the region by mid-afternoon on the 26th, so evaporation of hydrometeors did occur locally in showers, although much of the precipitation evaporated before reaching the ground. The flow was southwesterly throughout most of the column, the exception being at low levels at Denver where thunderstorm outflows affected the region (Section 5).

b. Satellite imagery

A sequence of two GOES-13 water vapor images 24 hours apart in the late afternoon on 25 and 26 June (0102 UTC on 26 and 27 June, respectively) is shown in Fig. 9. A plume of moisture extended northward along the Arizona-New Mexico border into eastern Utah/western Colorado on the 25th (Fig. 9a), and then into central Colorado on the 26th (Fig. 9b). The 6.5 μm water vapor channel has maximum weighting in the 300-500 hPa layer, so the axes of the GOES water vapor plumes do not coincide exactly (are displaced eastward in this case) with the positions of the moist tongues (Figs. 6c,d). The lines of storms that developed over central Utah at 0102 UTC on the 26th were linked most closely to the axis of the precipitable water maximum (Fig. 6c). Twenty-four hours later (Fig. 9b) the convection shifted to central Colorado, where it was tightly aligned along the rather narrow upper-tropospheric water vapor plume.

5. Mesoanalysis of convective systems on June 26

The convective system that eventually impacted the Waldo Canyon Fire first formed over the San Juan Mountains in southwestern Colorado at midday on the 26th (Fig. 10). As this sequence of visible images shows, over a six-hour period, the convective area grew in size and moved northeastward, passing to the northwest of Colorado Springs. As will be seen, even though the storm did not pass directly over Colorado Springs, the downdraft outflow from it had a major impact on the evolution of the fire.

As the convective system over the San Juan Mountains grew in size and moved northeastward (Fig. 10), by 2100 UTC (Fig. 11a) it produced a pronounced convective outflow with a leading gust front (labeled GF1) at the surface. Although radar beam blockage is a problem in this part of Colorado (Maddox et al. 2002), a cluster of convective cells was clearly evident at 2100 UTC, as was another area of convection and associated gust front (GF2) to the west of Denver (northern part of analysis domain). Over the next two hours (Fig. 11a-c), GF1

expanded and moved northeastward with scattered convection at its leading edge, reaching a position at 2300 UTC where it just began to impact the Waldo Canyon fire. GF2, on the other hand, moved southeastward, although it was still well north of the Colorado Springs area. At 0000 UTC on 27 June (Fig. 11d), GF1 had passed the fire and a sudden shift in direction and amplification of the smoke plume can be seen. The estimated average speed of the gust front GF1 over the three-hour period is 15 m s^{-1}. GF2 remained north of the Waldo Canyon fire at 0000 UTC.

Meteograms based on 5-min ASOS data for Centennial Airport (APA) and Colorado Springs (COS) (Fig. 12, see Fig. 4 for locations) indicate the GF1 passage, a sudden shift to strong westerlies (with a gust to 23 m s^{-1} at APA) between 2300 UTC on the 26th and 0000 UTC on the 27th. At APA (Fig. 12a), GF1 passage was preceded by GF2 passage between 2100 and 2200 UTC, although GF2 never reached COS (Fig. 12b) prior to GF1's arrival. However, a new outflow did appear to reach COS between 0100 and 0200 UTC after the passage of GF1 with a shift to north-northwesterly flow. Whether this wind shift was associated with GF2 or new convection that formed 20-30 km north of the fire at 0000 UTC (Fig. 11) is unclear. GF1 arrived at Pueblo (PUB) around 0030 UTC. At the Air Force Academy, located just north of Colorado Springs and on the northern perimeter of the fire (Fig. 2), there was a wind shift from southeasterly at 2300 UTC to west-northwesterly at 2302 UTC with gusts to 14 m s^{-1} and accompanied by a light shower, temperature drop of 5°C, relative humidity increase from 5 to 30%, and 1 hPa pressure rise. Therefore, the arrival of GF1 around 2300 UTC indicated in the mesoanalysis (Fig. 11c) is corroborated by the Air Force Academy observations. At the time of the fire blowup, there were media reports of winds up to 65 mph (29 m s^{-1}), but those reports could not be confirmed. However, at Manchester, a RAWS station 40 km northwest of Colorado Springs (Fig. 4), a sustained wind of 37 mph (17 m s^{-1}) from the west-southwest was reported at 2300 UTC, with a gust to 59 mph (26 m s^{-1}) during the previous hour (precise time not known). Winds of this magnitude would clearly have a major impact on the development of the fire.

6. Radar observations of the gust front and fire

A sequence of radar reflectivity and radial velocity images from the Pueblo, Colorado, radar at one-hour intervals from 2300 UTC on 26 June to 0100 UTC on 27 June is shown in Fig. 13. The reflectivity image at 2300 UTC (Fig. 13a) shows the smoke plume moving off to the northeast carried by the southwesterly flow aloft. By 0000 UTC (Fig. 13b), the gust front had moved through the fire area, causing an intensification and eastward shift of the smoke plume. Some of the intensification of the fire at this time may have also been related to the normal diurnal cycle, i.e., the hottest and driest conditions and deepest boundary layer occurred in the mid-to-late afternoon thus aiding fire growth. An hour later, at 0100 UTC (Fig. 13c), further intensification of the smoke plume can be seen along with a continuing eastward shift as the gust front, marked by a thin reflectivity line, moved out onto the plains.

The passage of the gust front can be better seen in the Pueblo radial velocity images (Fig. 13d-f). A wind-shift line separating southwesterly (orange/yellow colors) from westerly or northwesterly (green colors) flow moved through the location of the fire at 2300 UTC (Fig. 13d) and then eastward as the smoke plume rapidly expanded. The speed of the wind-shift line in the fire plume determined from an animation of the velocity images was 16-17 m s^{-1}, which is close to the estimated speed of the gust front based on the surface mesoanalyses. Animations of the radar reflectivity and radial velocity from the Pueblo radar can be found at http://johnson.atmos.colostate.edu/waldo_canyon_fire. The peak inbound radial velocities in the plume at 0000 UTC (Fig. 13e) exceeded 15 m s^{-1} behind the gust-front boundary, which was well in excess of the lower-tropospheric winds at Denver at 0000 UTC (Fig. 8) and is indicative of convective outflow dynamics. Continued eastward progression of the gust front is also seen in the radial velocity field at 0100 UTC (Fig. 13f).

A zoomed-in radar reflectivity image centered on the fire at 2300 UTC is shown in Fig. 14, along with radar echo-top information. The fire plume extends off to the northeast while convective cells are scattered throughout the northwestern portion of the domain. Highest echo tops are near 11 km (∼35,000 ft), although Lang et al. (2013) indicate tops to 13 km

and higher around this time.

A rapid increase in the vertical extent of the fire is apparent from 2200 to 2230 UTC (Fig. 15a,b), somewhat before the time of the wind shift inferred from station data. This intensification of the fire may be related to diurnal heating cycle, well known to impact the growth of wildland fires (e.g., Fromm et al. 2010). Increased reflectivities aloft continue beyond to 2300 and 2330 UTC (Fig. 15c,d). This intensification of the fire was manifested in increased lightning activity reported by Lang et al. (2013), where they noted a first increase at 2310 UTC and a second stronger burst at 2345 UTC. Lang et al. (2013) point out that the only lightning activity with the Waldo Canyon Fire occurred around the time of the passage of the gust front on the afternoon of 26 June, supporting the idea that the arrival of the convective outflow was a significant contributor to the intensification of the fire.

The radial velocity field from the Pueblo radar varied little between 2200 and 2300 UTC (Fig. 15e-g), but a marked change is seen between 2300 and 2330 UTC (Fig. 15g,h). During this period, there is clear evidence of the gust front moving past the fire out onto the plains from a pronounced increase in low-level radar reflectivity and outbound (southerly) flow switching to inbound (westerly) flow in the lowest 2-3 km, the approximate depth of the convective outflow. As the gust front surged eastward during this later period, there is a suggestion that the southerly (outbound) velocities are scoured and lifted upward over the outflow itself (Fig. 15g,h).

The movement of the gust front out onto the plains is further depicted in a 3-D perspective over a 37-min period from 2301 to 2338 UTC in Fig. 16. Ashes and other debris from the fire are the source of the radar reflectivity and can be seen to quickly spread eastward in the lowest 3 km undercutting the smoke plume aloft. It is this rapid eastward advance of the low-level gust front that quickly spread the fire into the western suburbs of Colorado Springs.

7. Simulated convection and associated gust fronts

The WRF-ARF was run for 27 h starting at 0000 UTC 26 June and ending at 0300 UTC 27 June. The 27-h total precipitation for the simulation is shown in Fig. 17. An elongated zone of generally light precipitation is forecast in a band along the moisture plume (Fig. 9) extending from Arizona into the northern Plains.

Shown in Fig. 18a-d are a sequence of mesoanalyses from the simulation for this case for the period 2000 to 2300 UTC. For comparison purposes, these analyses of simulated radar reflectivity, surface winds, and surface potential temperature have been constructed over the same domain as the observed outflows in Fig. 11, though the timing for each panel is one hour earlier. The simulated storms that produced the precipitation across Colorado were mainly grouped into organized convective complexes with associated extensive surface downdraft outflows. In agreement with observations, the model produces two organized outflows and associated gust fronts (GF1 and GF2) that move from the mountains onto the eastern plains of Colorado. The largest discrepancy is that the timing of the gust front passage at the Waldo Canyon fire is approximately two hours too early (cf. Figs. 11 and 18). However, considering that the organized convective complexes and overall positions and shapes of both GF1 and GF2 are well simulated, it is evident that substantial predictability of the weather events that impacted the fire existed in the large-scale fields a day in advance.

Simulated vertical cross sections showing the passage of the GF1 down the slopes of the Rocky Mountain terrain are presented in Fig. 19a-d for the period 1900 to 2200 UTC. Once again, the timing of the passage of GF1 is approximately two hours earlier in the model than observed. As the gust front moves over the various ridges to the west of the fire, both the winds and potential temperature structures indicate the occurrence of hydraulic jumps on the downwind sides of individual barriers (Smith 1989). The existence of hydraulic jump in the vicinity of the fire could have not only intensified the downslope winds, but also lengthened the duration of the high winds.

Early on (Figs. 19a-c), the gust front has a relatively strong temperature gradient asso-

ciated with it (1900-2100 UTC), but by the time it reaches the fire (2200 UTC; Fig. 19d), the temperature gradient has weakened considerably. This weakening is likely related to the fact that the convection driving the outflow has mostly died out by this time and the cold pool has now moved far from its source. When the simulated cold pool reached the fire (Fig. 19c), its depth was approximately 2 km, which is roughly consistent with the observations shown in Fig. 14. Animations of the simulation results shown in Figs. 18 and 19 can be found at http://johnson.atmos.colostate.edu/waldo_canyon_fire.

8. Summary and conclusions

This paper examines the meteorological conditions accompanying the catastrophic Waldo Canyon Fire of June 2012 in the Colorado Springs area. The fire occurred following one of the driest and warmest winter and spring periods in recorded history over the Intermountain West. In terms of economic loss, the Waldo Canyon Fire was the most destructive forest fire on record in Colorado. While property loss was staggering, the quick action of emergency management teams saved the lives of many citizens living in the path of the fire.

On the afternoon of June 26, the Waldo Fire rapidly intensified and quickly advanced into a densely populated neighborhood in the northwest part Colorado Springs, destroying nearly 350 homes. Mesometeorological analyses of the event show that rapidly changing weather conditions played a key role in the blow-up and sudden advance of the fire during the afternoon. Specifically, based on surface observations from a variety of surface stations over Colorado, as well as numerical simulations, evidence is presented to show that the explosive growth of the fire was timed with the afternoon passage of a strong gust front across the region. The gust front had its origins within a thunderstorm complex that formed during midday over the San Juan mountains of southwestern Colorado.

The synoptic-scale setting on 26 June featured a strong upper-level high over the central United States with relatively weak southwesterly flow over Colorado. On a the preceding

day, a tongue of moist air emanating from northwestern Mexico streamed into southern Utah leading to afternoon thunderstorms in that state. That moisture plume shifted eastward to Colorado on the 26th and along with very dry conditions in the lower troposphere, created ideal conditions for high-based thunderstorms accompanied by microbursts (Wakimoto 1985). Indeed, the thunderstorms that first formed at midday over southwestern Colorado, upon moving to the south-central part of the state, produced an organized convective downdraft outflow that moved eastward at about 15 m s^{-1}, arriving at the location of the Waldo Fire at about 2300 UTC (1700 LT). Coupled with the maximum daytime heating, the gust front passage led to a blowup and rapid expansion of the fire boundary (Figs. 1 and 2). Radar analysis demonstrates that this expansion coincided with rapid deepening and intensification of the smoke plume. The sudden intensification of the fire by the gust front is further substantiated by bursts of lightning activity occurring around the same time, the only incidence of lightning during the fire's existence (Lang et al. 2013). A secondary cold pool and gust front occurred to the north of Colorado Springs, but it did not reach the location of the fire.

Numerical simulations of the event using a 4-km version of the Advanced WRF (ARW) starting with initial conditions one day earlier produced a very realistic representation of the sequence of events on this day. The model successfully simulated the gust front that passed over the fire as well as the second outflow to north, although the timing was approximately two hours too early. The overall dimensions and structure of the outflow systems agreed very well with the observations. The modeled vertical structure of the gust front affecting the fire showed it to be a ∼2-3 km deep cold pool with a temperature contrast at its leading edge weakening with time as it moved eastward away from the convective source region. As the cold pool passed over ridges along the sloped terrain on the east slopes of the Rocky Mountains, it produced hydraulic jumps to the lee of individual barriers. From the results of the simulations, it is concluded that a considerable degree of predictability of high-based convection and associated macroburst-driven outflows that impacted the Waldo Canyon

Fire existed in the large-scale conditions over the west-central United States at least a day in advance.

Acknowledgments.

This research has been supported by the National Science Foundation under Grants AGS-1059899 and AGS-1157425. We acknowledge Black Ice Geospatial for the fire boundary locations in Fig. 2. The views, opinions, and findings in this report are those of the authors, and should not be construed as an official NOAA and or U.S. Government position, policy, or decision.

REFERENCES

Butler, B. W., R. A. Bartlette, L. S. Bradshaw, J. D. Cohen, P. L. Andrews, T. Putnam, and R. J. Mangan, 1998: Fire behavior associated with the 1994 South Canyon Fire on Storm King Mountain, Colorado. Research Paper RMRS-RP-9, United States Forest Service, Rocky Mountain Research Station, 81 pp.

Clark, T. L., M. A. Jenkins, J. Coen, and D. Packham, 1996: A coupled atmospherefire model: convective feedback on fire-line dynamics. *J. Appl. Meteor.*, **35**, 875–901.

Clark, T. L., L. Radke, and D. Middleton, 1999: Analysis of small-scale convective dynamics in a crown fire using infrared video cameras. *J. Appl. Meteor.*, **38**, 1401–1420.

Cunningham, P. and M. J. Reeder, 2009: Severe convective storms initiated by intense wildfires: numerical simulations of pyro-convection and pyro-tornadogenesis. *Geophys. Res. Lett.*, **36**, doi:10.1029/2009GL039262.

Diaz, H. F. and T. W. Swetnam, 2013: The wildfires of 1910: Climatology of an extreme early twentieth-century event and comparison with more recent events. *Bull. Amer. Meteor. Soc.*, **94**, 1361–1370.

Engel, C. B., T. P. Lane, M. J. Reeder, and M. Rezny, 2012: The meteorology of Black Saturday. *Quart. J. Roy. Meteor. Soc.*, **139**, 585–599.

Fromm, M., D. T. Lindsey, R. Servranckx, G. Yue, T. Trickl, R. Sica, P. Doucet, and S. Godin-Beekman, 2010: The untold story of pyrocumulonimbus. *Bull. Amer. Meteor. Soc.*, **91**, 1193–1209.

Fujita, T. T., 1985: *The Downburst*. The University of Chicago, 122 pp.

412 Gilmore, M. S. and L. J. Wicker, 1998: The influence of midtropospheric dryness on supercell
413 morphology and evolution. *Mon. Wea. Rev.*, **126**, 943–958.

414 Goens, D. W. and P. L. Andrews, 1998: Weather and fire factors related to the 1990 Dude
415 Fire near Payson, Arizona. *Extended Abstracts, Second Symposium on Fire and Forest*
416 *Meteorology*, Phoenix, AZ, Amer. Meteor. Soc., 153–158.

417 Horel, J., et al., 2002: Mesowest: Cooperative mesonets in the Western United States. *Bull.*
418 *Amer. Meteor. Soc.*, **83**, 211–225.

419 Iacono, M. J., J. S. Delamere, E. J. Mlawer, M. W. Shephard, S. A. Clough, and W. D.
420 Collins, 2008: Radiative forcing by long-lived greenhouse gases: Calculations with the
421 AER radiative transfer models. *J. Geophys. Res.*, **113**, doi:10.1029/2008JD009944.

422 Janjić, L., 2002: Nonsingular implementation of the Mellor-Yamada level 2.5 scheme in the
423 NCEP Meso model. NCEP Office Note 437, National Centers for Environmental Predic-
424 tion, 61 pp.

425 Kiefer, M. T., M. D. Parker, and J. J. Charney, 2009: Regimes of dry convection above
426 wildfires: Idealized numerical simulations and dimensional analysis. *J. Atmos. Sci.*, **66**,
427 806–836.

428 Kuchera, E. L. and M. D. Parker, 2006: Severe convective wind environments. *Wea. Fore-*
429 *casting*, **21**, 595–612.

430 Lang, T. J., S. A. Rutledge, B. Dolan, P. Krehbiel, W. Rison, and D. T. Lindsey, 2013:
431 Lightning in wildfire smoke plumes observed in Colorado during summer 2012. *Mon. Wea.*
432 *Rev.*, (in press).

433 Maddox, R. A., J. Zhang, J. J. Gourley, and K. W. Howard, 2002: Weather radar coverage
434 over the contiguous United States. *Wea. Forecasting*, **17**, 927–934.

435 Meister, M., 2013: The Waldo Canyon Fire: Communication successes and challenges as the
436 station scientist. *Abstracts, Impacts: Weather 2012*, Austin, TX, Amer. Meteor. Soc.

437 Mellor, G. L. and T. Yamada, 1982: Development of a turbulence closure model for geo-
438 physical fluid problems. *Rev. Geophys.*, **20**, doi:10.1029/RG020i004p00851.

439 Morrison, H., J. A. Curry, and V. I. Khvorostyanov, 2005: A new double-moment micro-
440 physics scheme for application in cloud and climate models. Part I: Description. *J. Atmos.*
441 *Sci.*, **62**, 1665–1677.

442 Myrick, D. and J. Horel, 2008: Sensitivity of surface analyses over the western United States
443 to RAWS observations. *Wea. Forecasting*, **23**, 145–158.

444 Potter, B. E., 2012a: Atmospheric interactions with wildland fire behavior – I. Basic surface
445 interactions, vertical profiles and synoptic structures. *Inter. J. Wildland Fire*, **21**, 779–801.

446 Potter, B. E., 2012b: Atmospheric interactions with wildland fire behavior – II. Plume and
447 vortex dynamics. *Inter. J. Wildland Fire*, **21**, 802–817.

448 Skamarock, W. C., et al., 2008: A description of the Advanced Research WRF Version 3.
449 NCAR Tech. Note NCAR/TN-475+STR, National Center for Atmospheric Research, 125
450 pp.

451 Smith, R. B., 1989: Hydrostatic air-flow over mountains. *Adv. Geophys.*, **31**, 1–41.

452 Stark, J., 2013: NWS decision support services before, during and AFTER the Waldo
453 Canyon Wildfire. *Abstracts, Impacts: Weather 2012*, Austin, TX, Amer. Meteor. Soc.

454 Steenburgh, W. J., C. R. Neuman, G. L. West, and L. F. Bosart, 2009: Discrete frontal
455 propagation over the Sierra-Cascade mountains and Intermountain West. *Mon. Wea. Rev.*,
456 **137**, 2000–2020.

457 Taylor, R. J., S. J. Evans, N. K. King, E. T. Stephens, D. R. Packham, and R. G. Vines,
458 1973: Convective activity above a large-scale bushfire. *J. Appl. Meteor.*, **12**, 1144–1150.

Wakimoto, R. M., 1985: Forecasting dry microburst activity over the High Plains. *Mon. Wea. Rev.*, **113**, 1131–1143.

Werth, P. A., et al., 2011: Synthesis of knowledge of extreme fire behavior: Volume I for fire managers. USDA General Tech. Rep. PNW-GTR-854, United States Forest Service, Pacific Northwest Research Station, 144 pp.

List of Figures

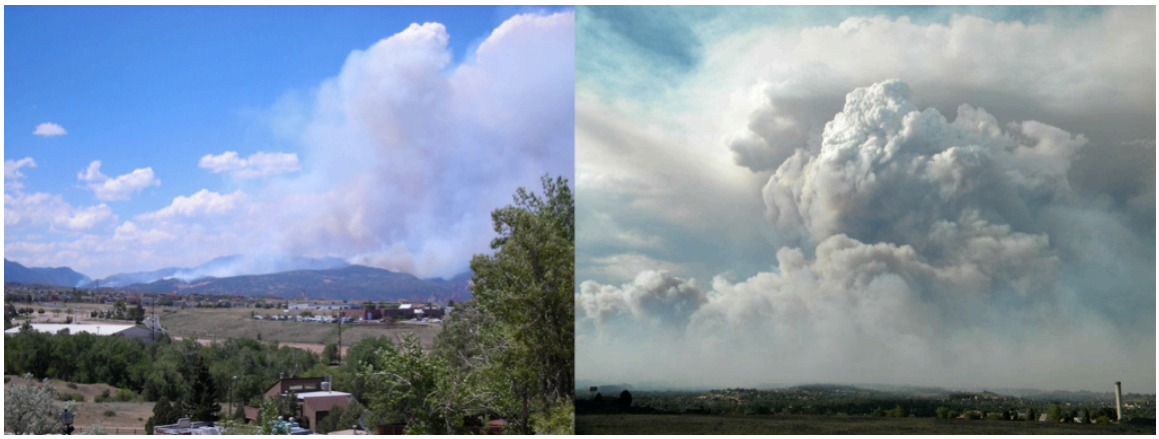

FIG. 1. Waldo Canyon Fire on June 26 during (left) early afternoon from above 8th Street in Colorado Springs (source: Dr. frog/Wikimedia Commons), and (right) late afternoon/early evening from southwest of Colorado Springs (source: www.senmwx.com). Pyrocumulonimbus was evident during the height of the fire.

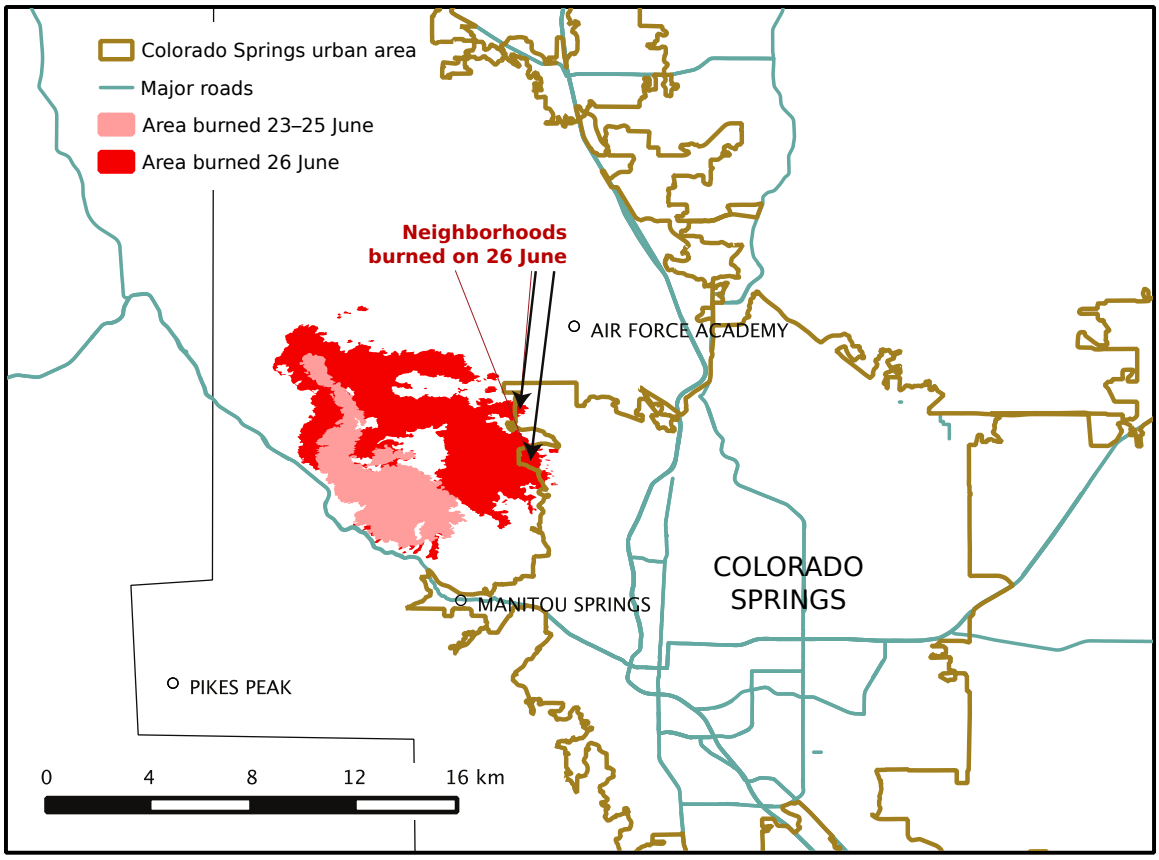

FIG. 2. Map showing rapid expansion of Waldo Canyon Fire area on 26 June 2012 beyond previous area into western Colorado Springs. Brown lines denote Colorado Springs city limits and blue lines major highways.

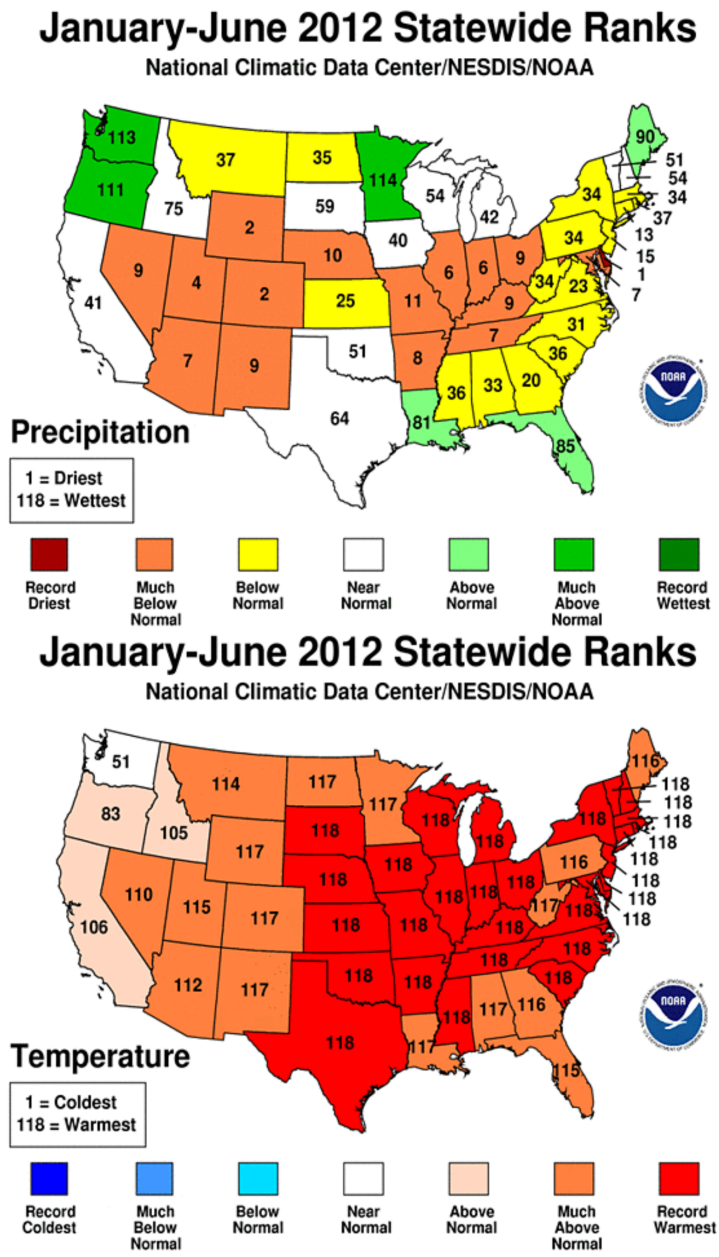

FIG. 3. January-June 2012 statewide average (top) precipitation and (bottom) temperature rankings. From these, it can be seen that this period was the second driest and warmest in recorded Colorado history.

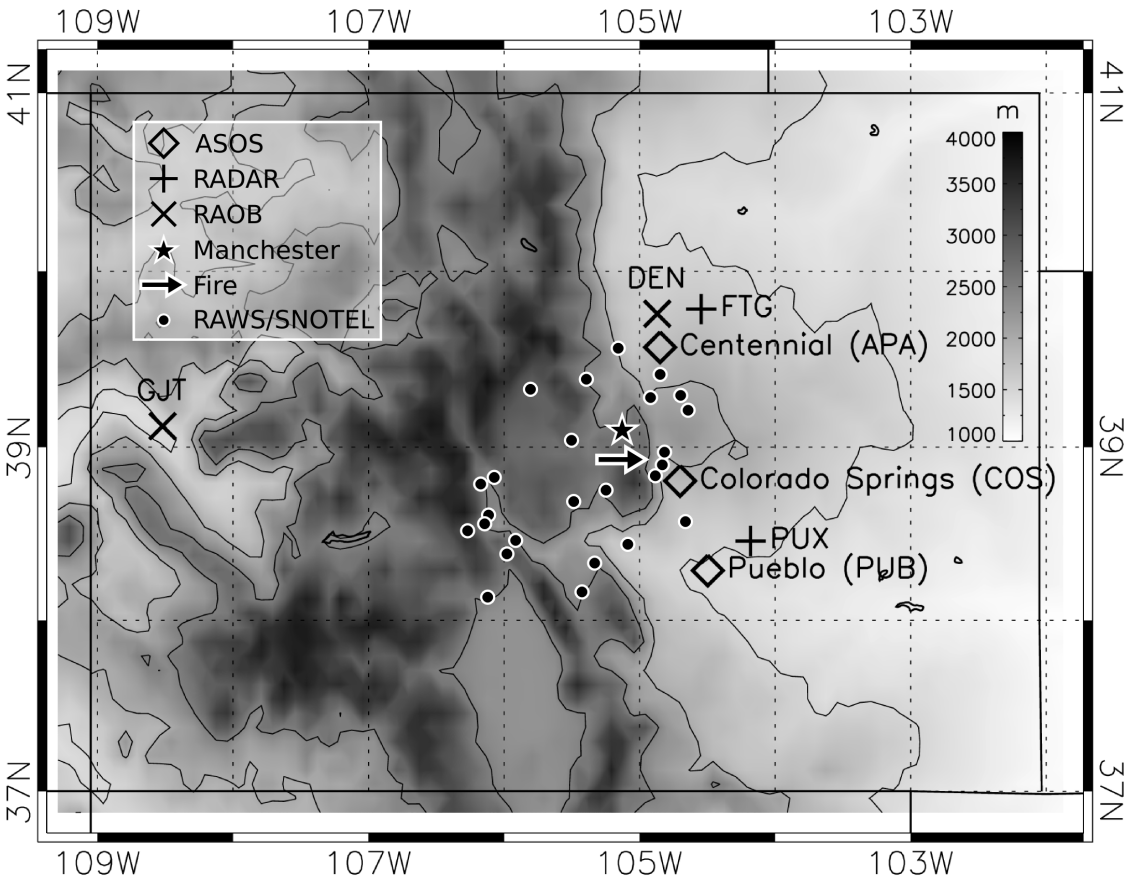

FIG. 4. NWS radar, ASOS, and sounding (RAOB) sites used in the analysis of convection and associated gust fronts over Colorado. Dots designate RAWS and SNOTEL sites used in the mesoanalyses. Elevation contours in m.

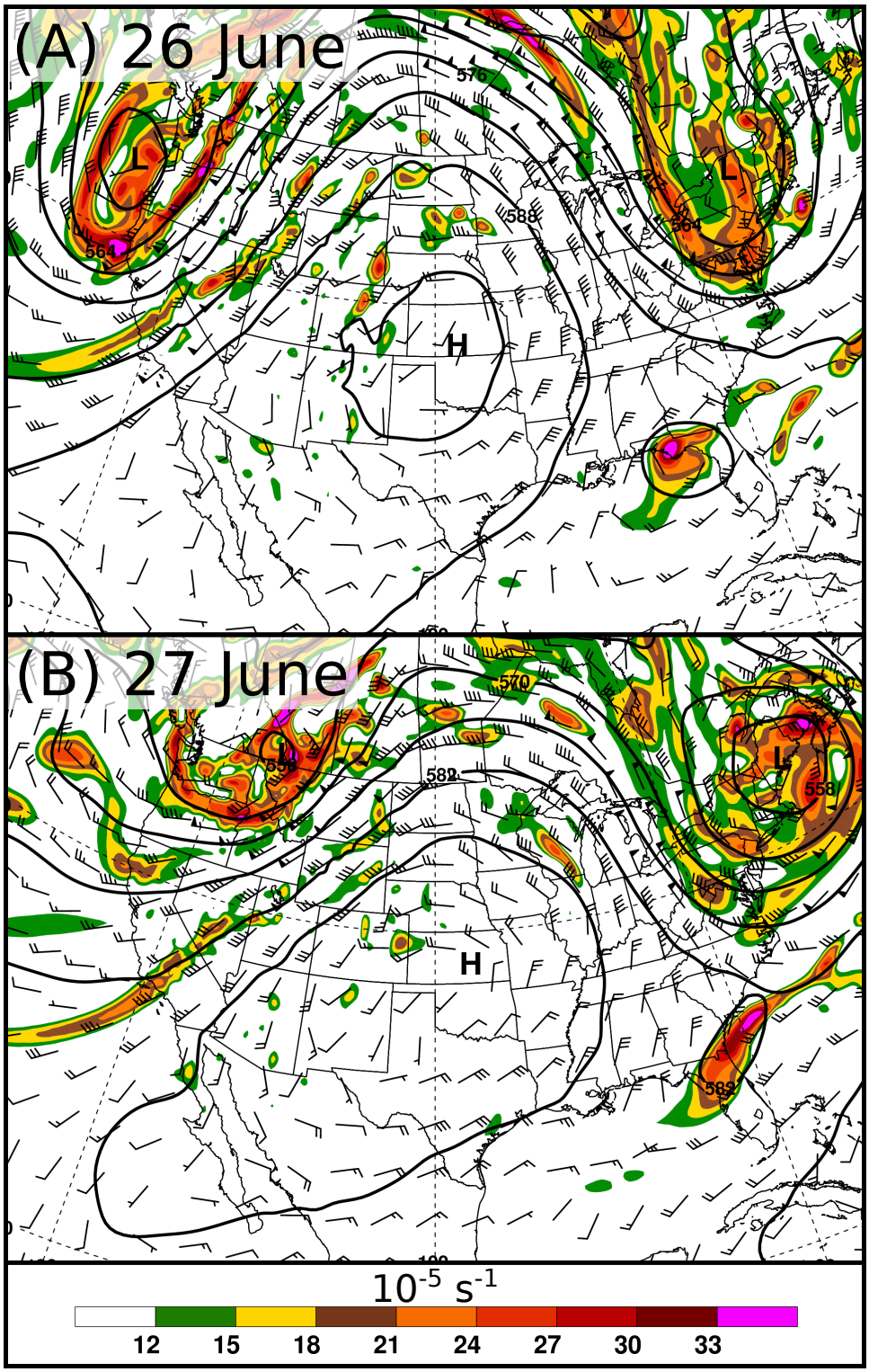

FIG. 5. Heights (contours, dam), absolute vorticity (shaded, 10^{-5} s^{-1}), and winds (flag = 25 m s^{-1}, full barb = 5 m s^{-1}, and half barb = 2.5 m s^{-1}) at 500 hPa at 0000 UTC on (a) 26 June and (b) 27 June based on GFS analysis.

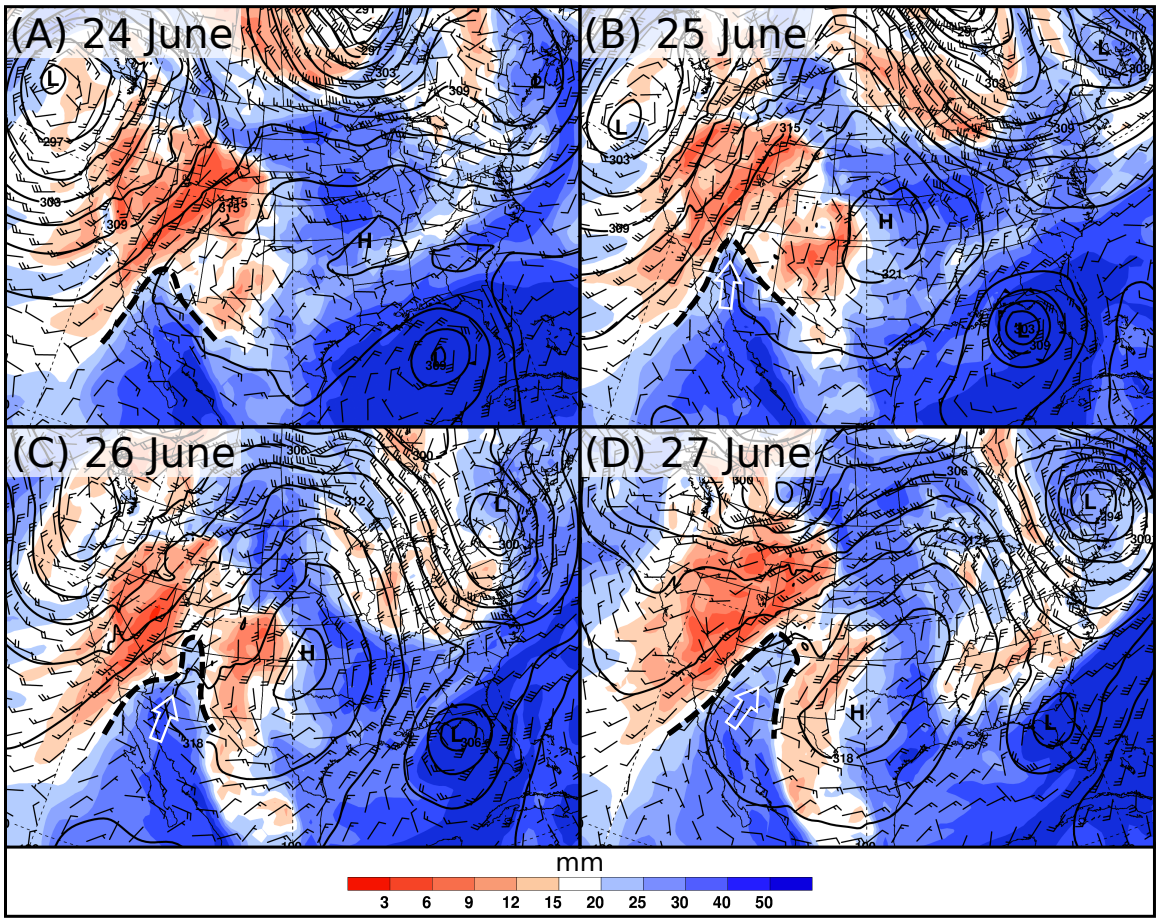

FIG. 6. 700 hPa heights (contours, dam), winds, and precipitable water (mm) at 0000 UTC on 24-27 June (a)-(d). Dashed line shows approximate position of 20 mm contour. Arrow indicates direction of moisture transport.

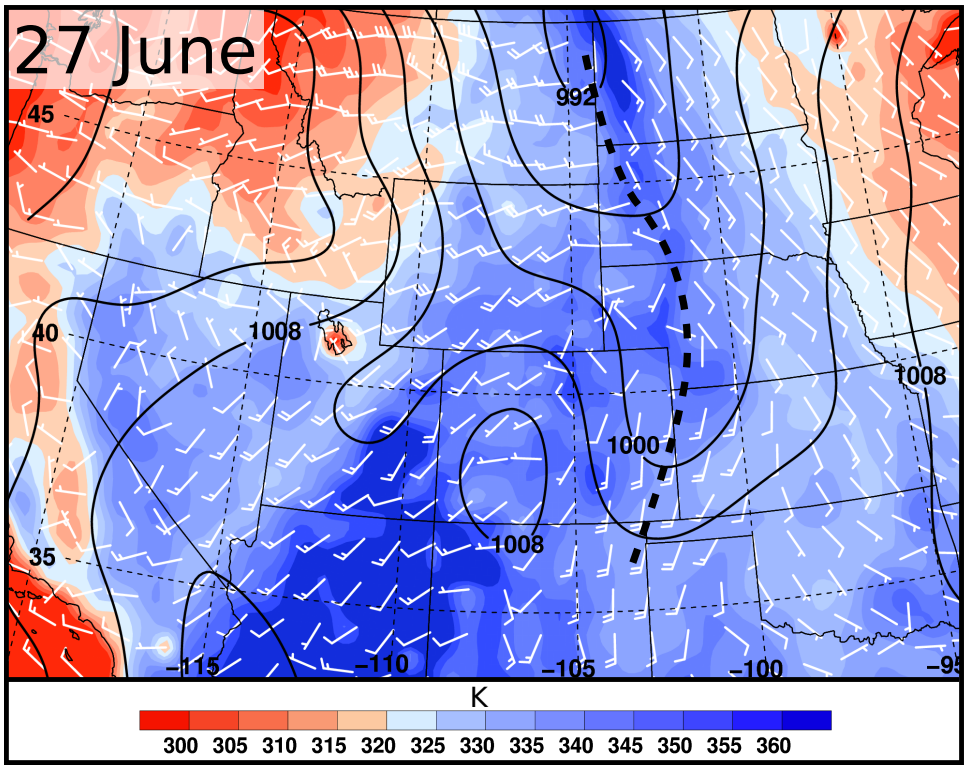

FIG. 7. Surface pressure (contours, hPa), winds, and equivalent potential temperature (color, K) at 0000 UTC 27 June.

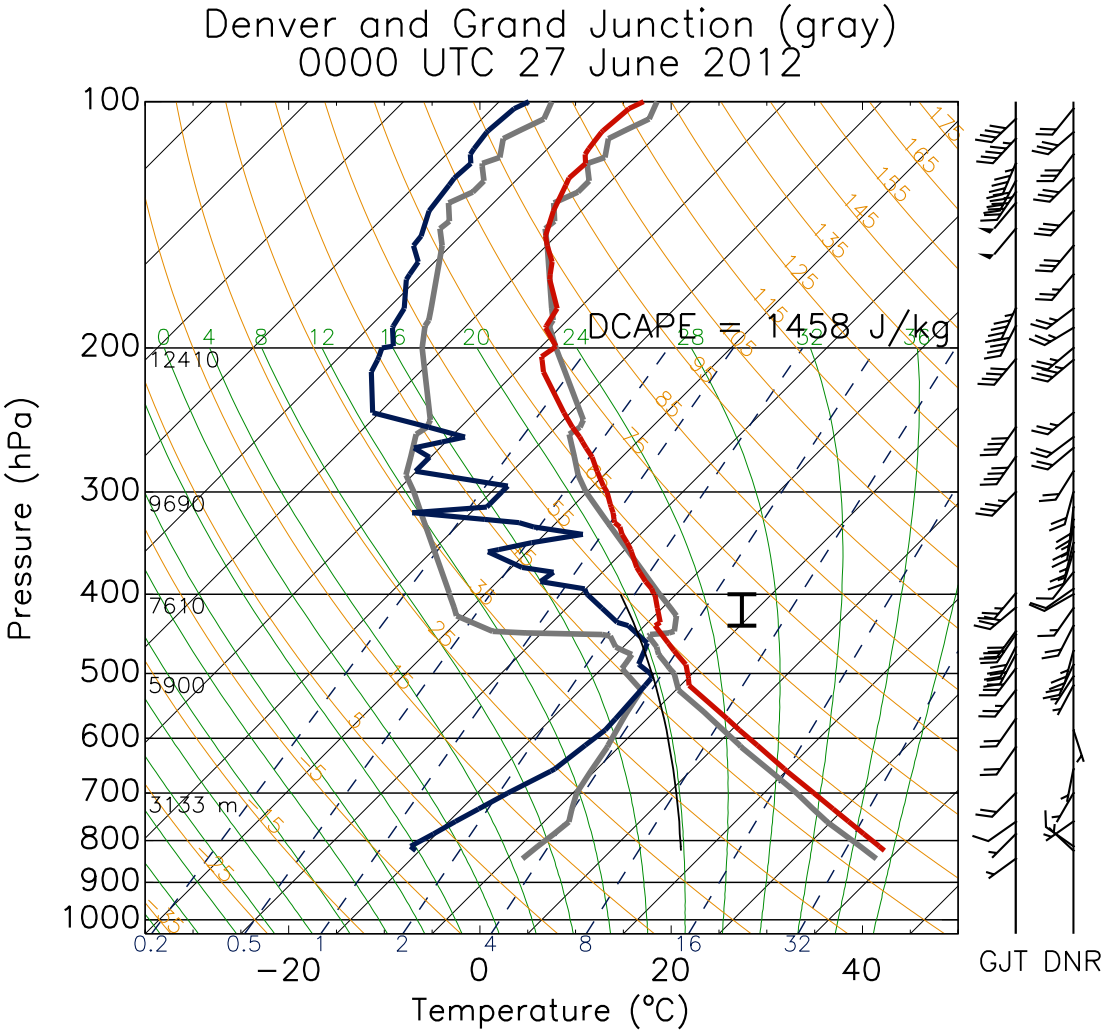

FIG. 8. Soundings from Denver (DNR) and Grand Junction (GJT), Colorado, at 0000 UTC, 27 June 2012. Downdraft available potential energy (DCAPE, computed for the vertical interval denoted in the plot) for DNR is indicated.

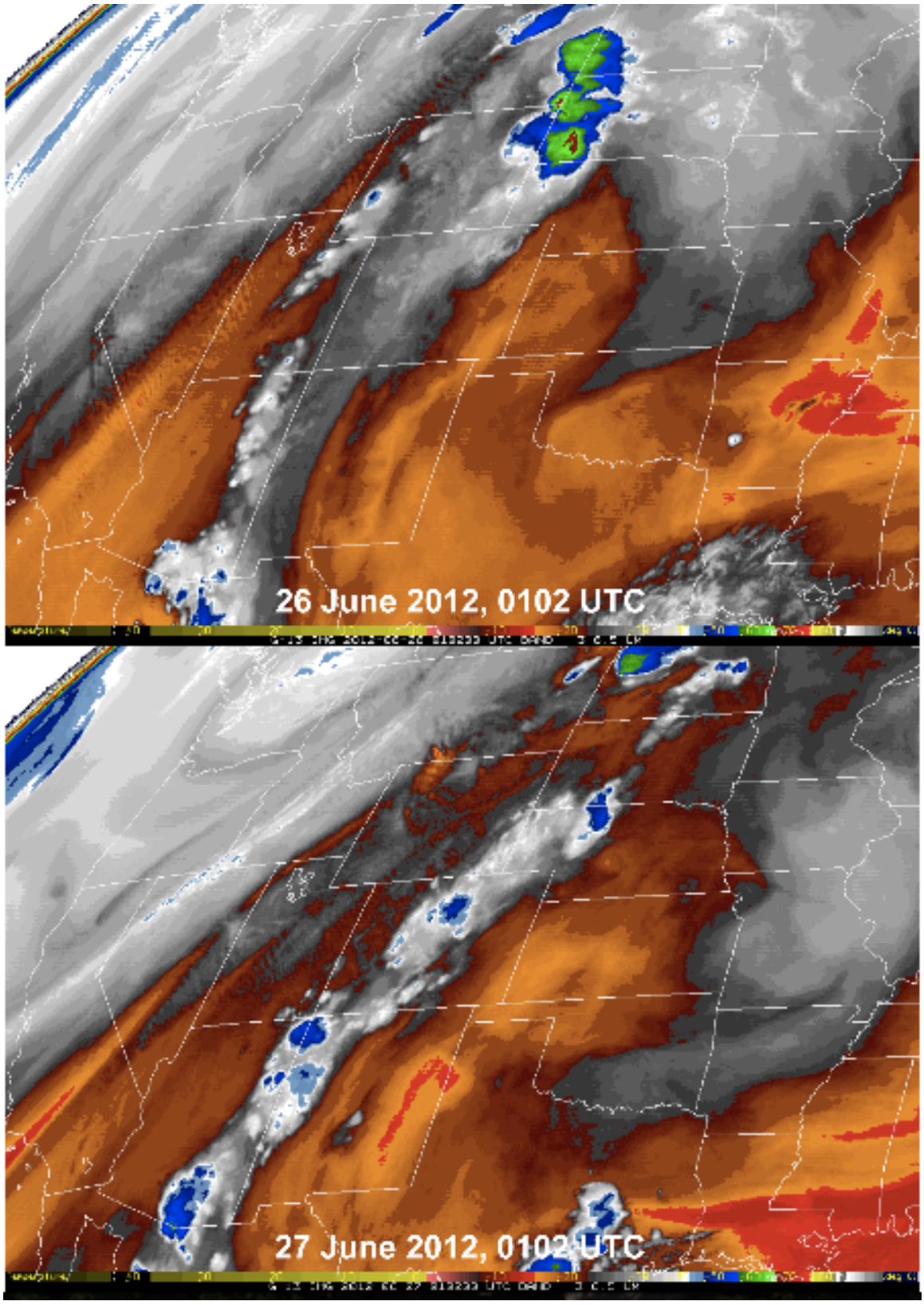

FIG. 9. GOES-13 water vapor imagery for 0102 UTC, 26 and 27 June 2012

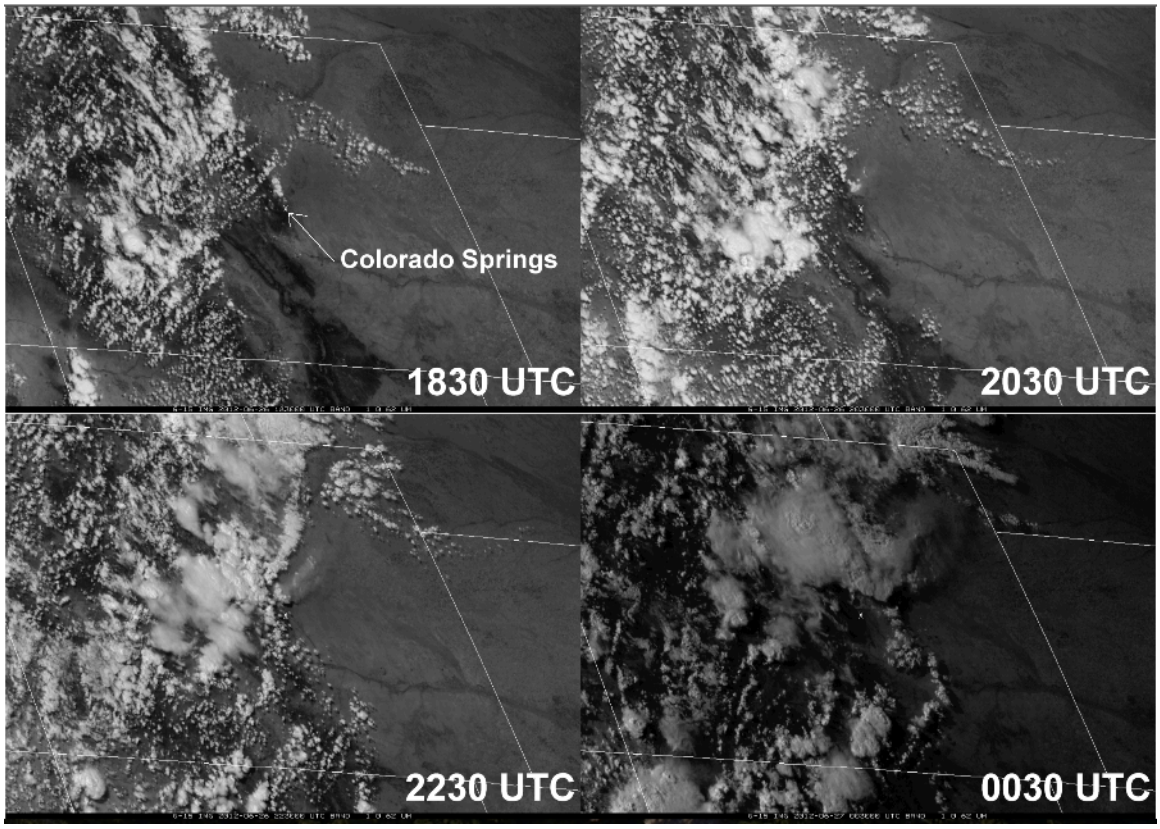

FIG. 10. GOES-15 visible imagery at 1830, 2030, and 2230 UTC on 26 June and 0030 UTC on 27 June 2012.

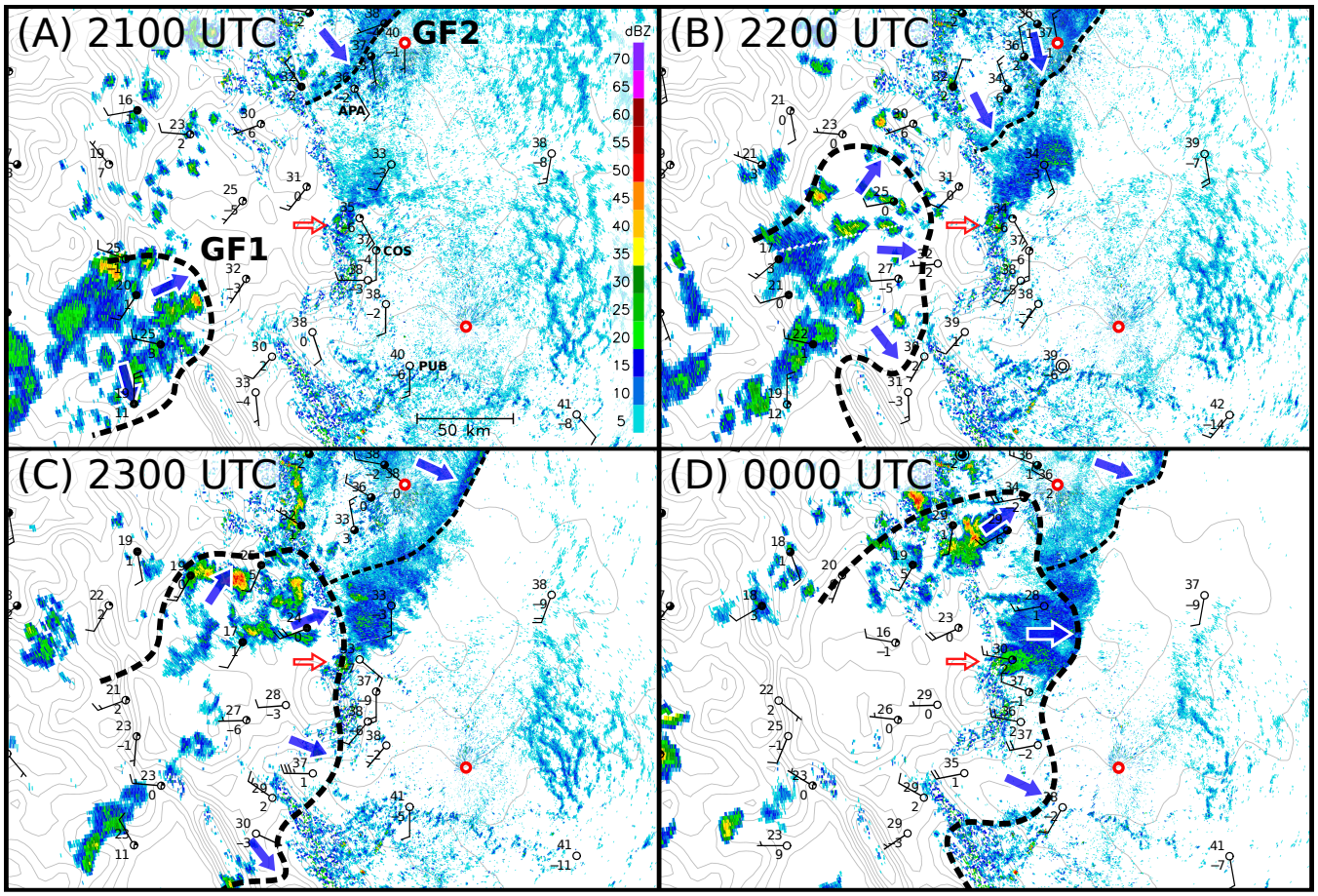

FIG. 11. Winds, temperature and dew point (°C), and mosaic base radar reflectivity for the periods (a) 2100, (b) 2200, (c) 2300 UTC on 26 June and (d) 0000 UTC 27 June. Two gust front (GF1 and GF2) positions (dashed lines) are located based on high time resolution data from surface stations and radar reflectivity and velocity data from Denver (FTG) and Pueblo (PUX) radars (red circles). See Fig. 4 for locations of stations. Red arrow points to Waldo Canyon Fire, blue arrows indicate direction of surface flow. Locations of meteogram sites (APA, COS, and PUB) in Fig. 12 are indicated in 2100 UTC panel. Terrain interval 200 m.

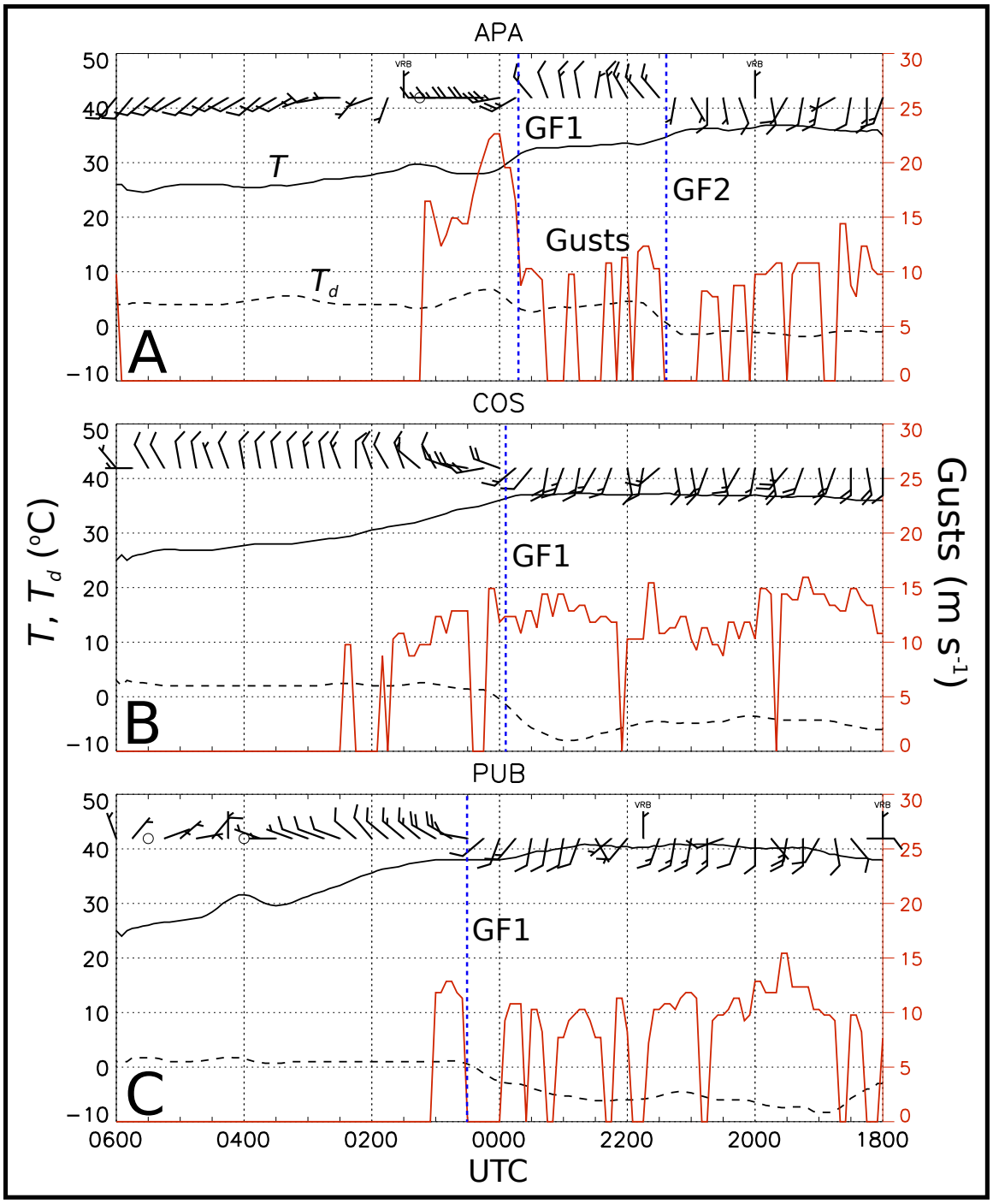

FIG. 12. Meteograms of winds, temperature and dew point (°C), and peak wind gusts (m s^{-1}) at (a) Centennial (APA), (b) Colorado Springs (COS), and (c) Pueblo (PUB) from 1800 UTC 26 June to 0600 UTC 27 June 2012. See Fig. 4 for station locations. Vertical lines mark times of GF1 and GF2 passage.

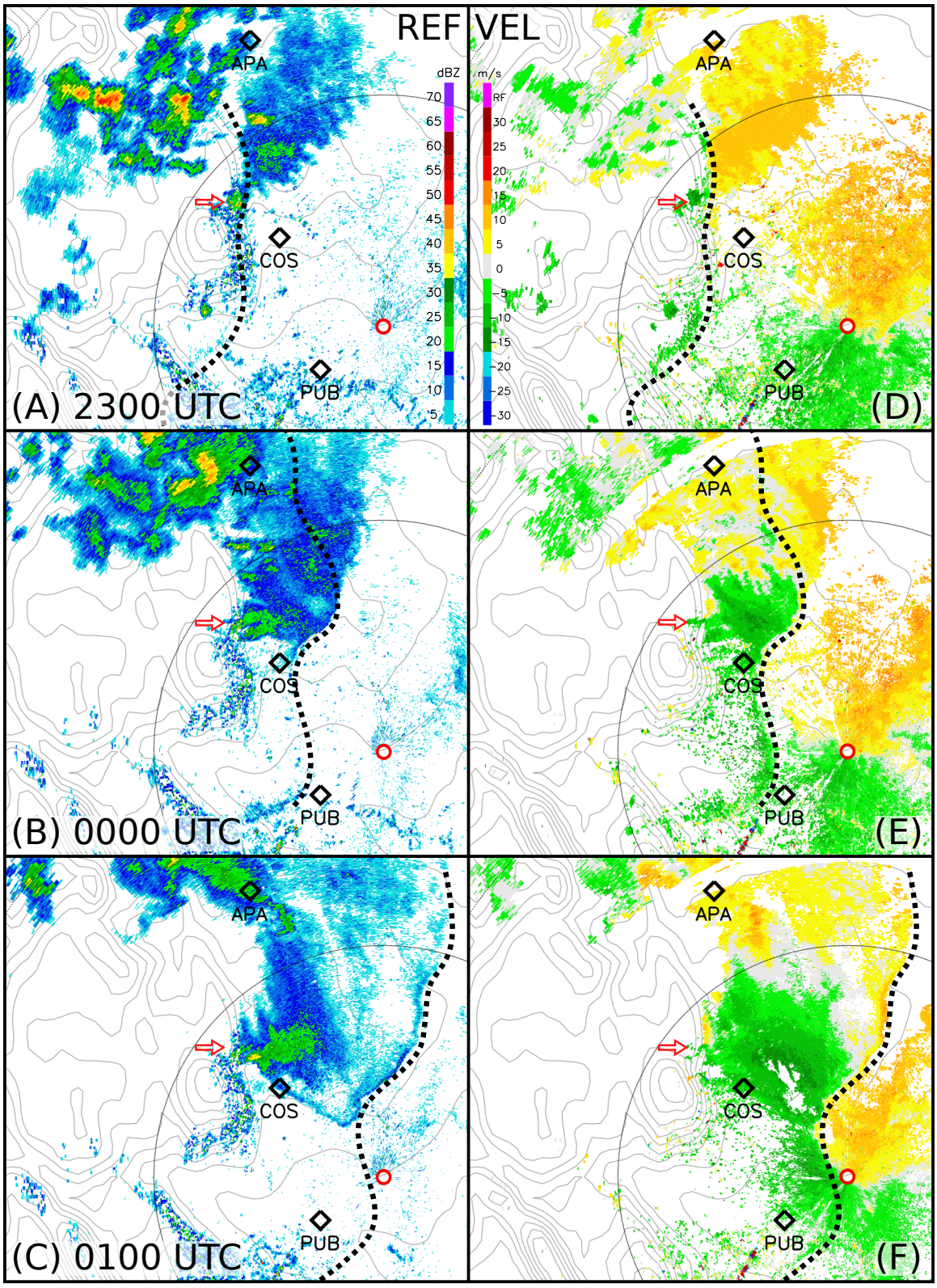

FIG. 13. Sequence of (a-c) base radar reflectivity and (d-f) radial velocity images from Pueblo, Colorado, WSR-88D radar (red circle) from 2300 UTC 26 June to 0100 UTC 27 June 2012. Red arrow denotes location of Waldo Canyon Fire. Gust front positions are indicated by dotted line. Range rings are at 100 km intervals, terrain interval is 200 m.

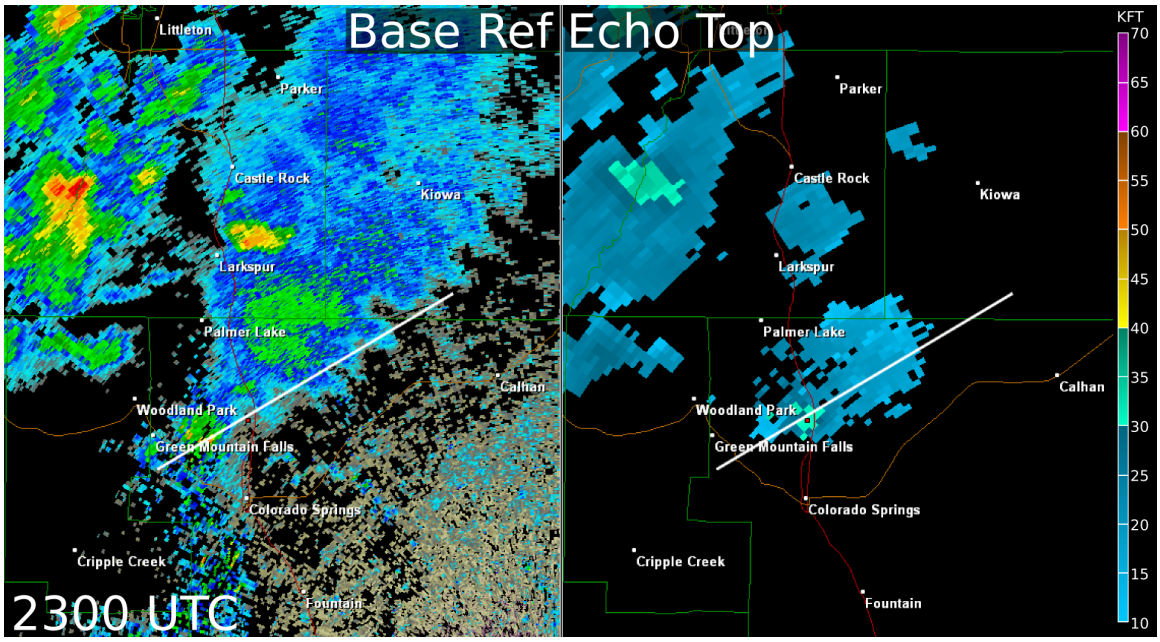

FIG. 14. (left) Radar reflectivity plot (same scale as in Fig. 11) centered over fire plume and (right) radar echo tops (scale on right) at 2300 UTC 26 June. White line denotes location of transect in Fig. 15.

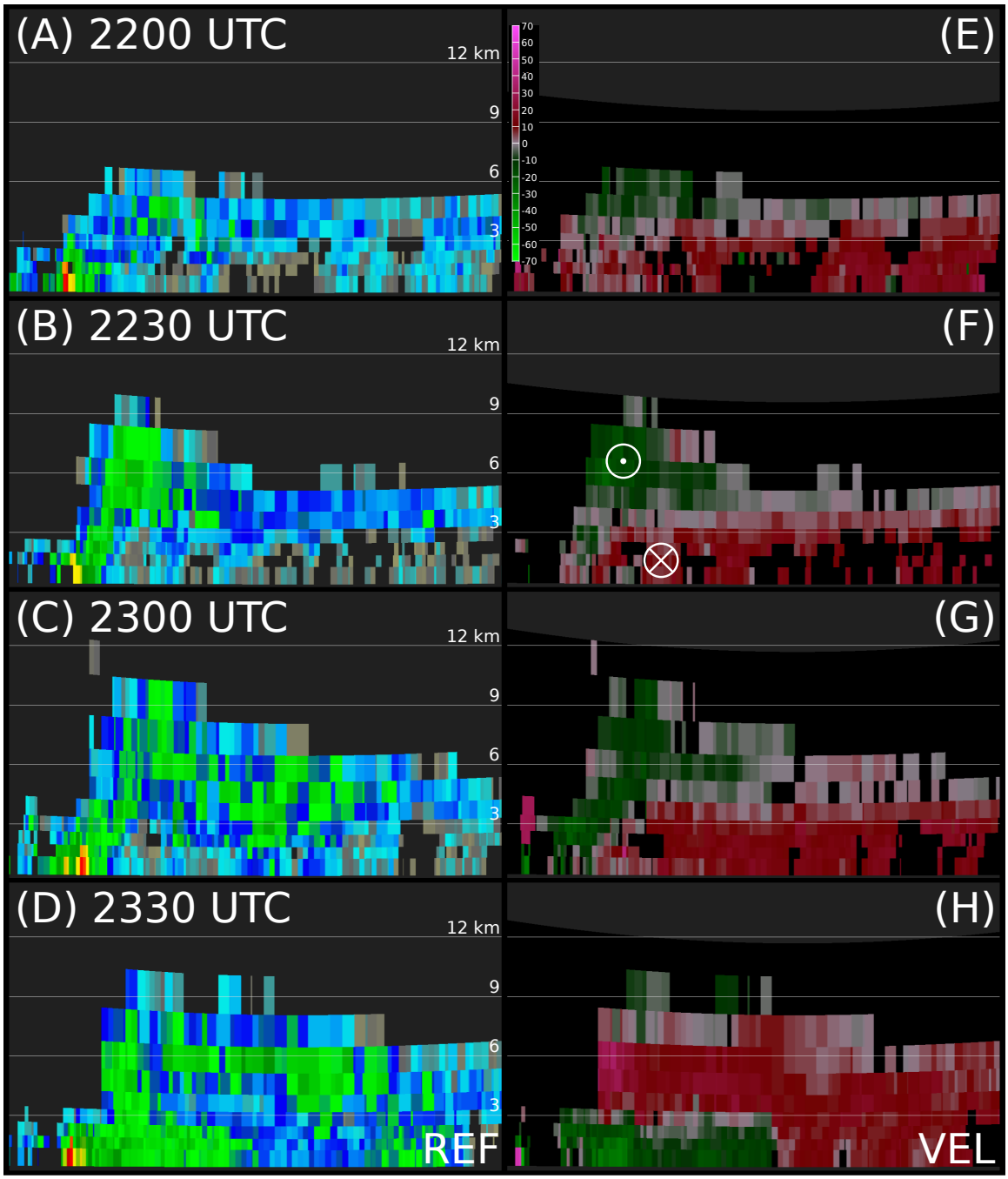

FIG. 15. Vertical cross sections of (a-d) radar reflectivity (same scale as in Fig. 14) and (e-h) radial velocity (m s^{-1}) based on Pueblo (PUX) radar from 2200 to 2330 UTC 26 June. Heights are distances above ground level. Circled dot (cross) denotes flow into (out of) the page.

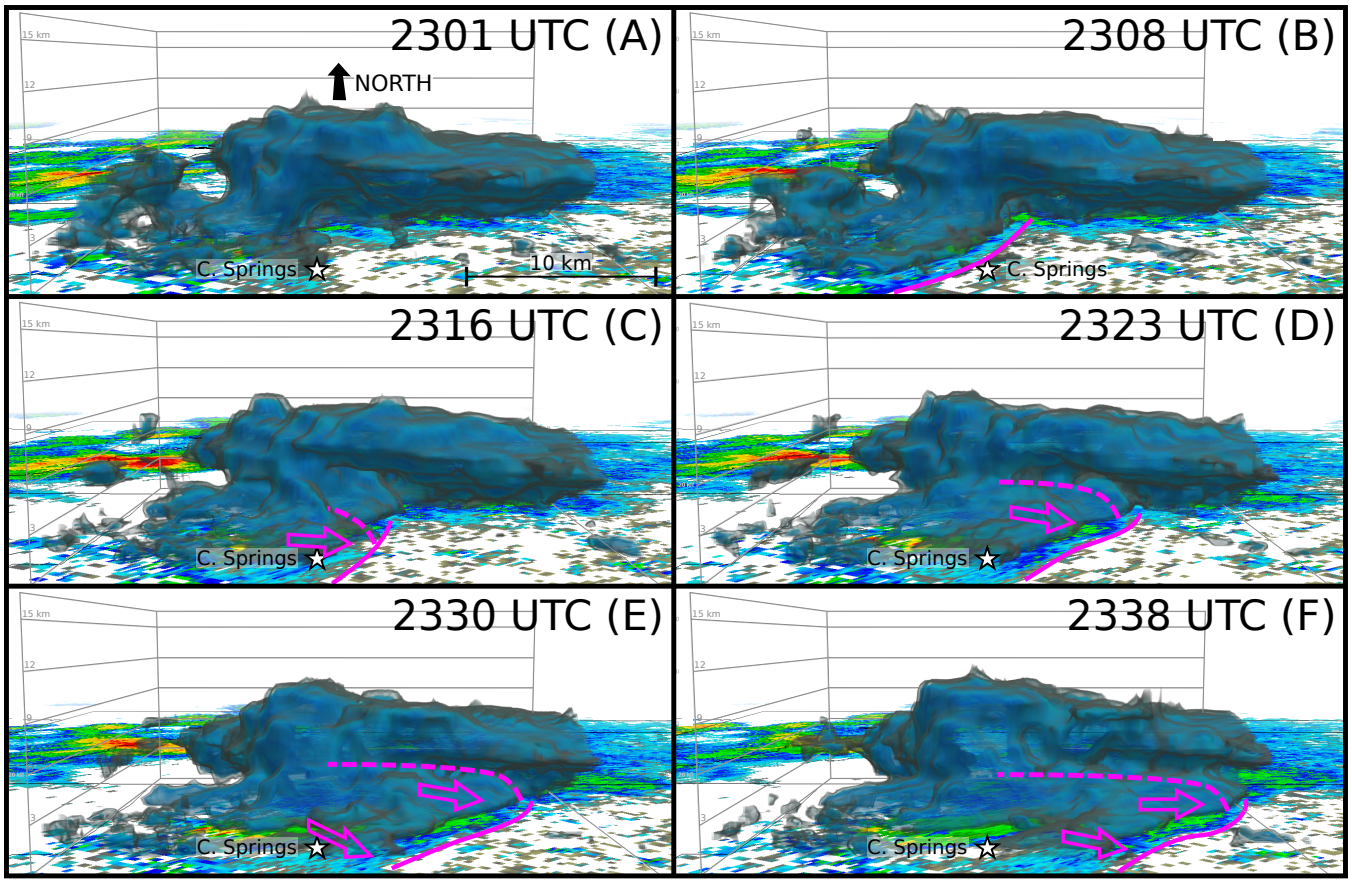

FIG. 16. Three-dimensional depictions of radar reflectivity at ∼7-min intervals from (a-f) 2301 to 2338 UTC 26 June from Pueblo WSR-88D radar. Approximate position of low-level gust-front boundary is indicated. Two shells of reflectivity are highlighted: −2 to +2 dBZ for gray outer shell, 7-12 dBZ for blue shell.

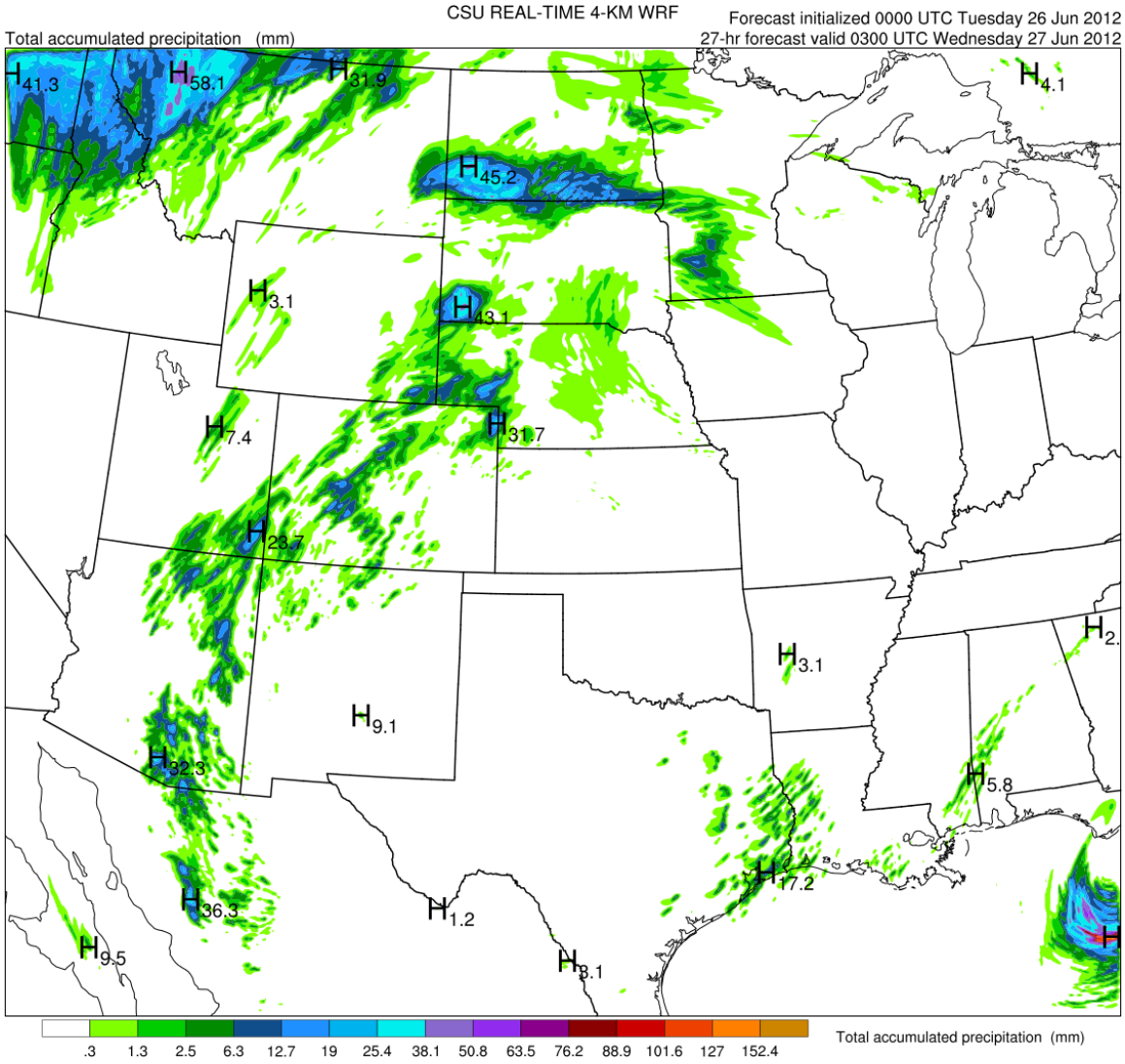

FIG. 17. Twenty-seven hour total precipitation (mm) for WRF-ARW forecast starting at 0000 UTC 26 June 2012.

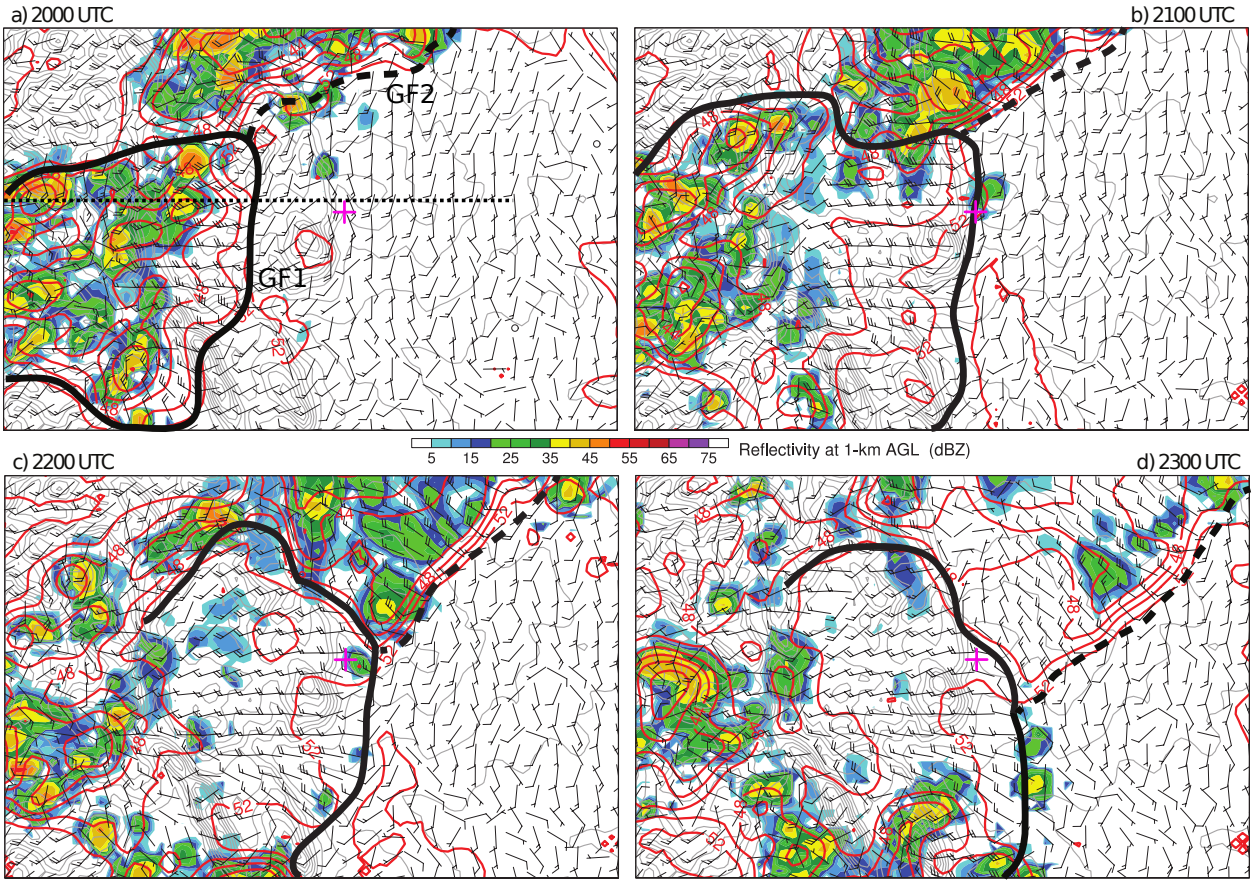

FIG. 18. Simulated radar reflectivity at 1-km AGL and surface winds, and potential temperature (2 °C interval) from (a-d) 2000 to 2300 UTC, 26 June 2012. Terrain interval is 200 m. Two gust fronts (GF1 and GF2) are indicated. Plus denotes location of Waldo Canyon Fire. Dotted line in (a) indicates position of vertical cross section in Fig. 19.

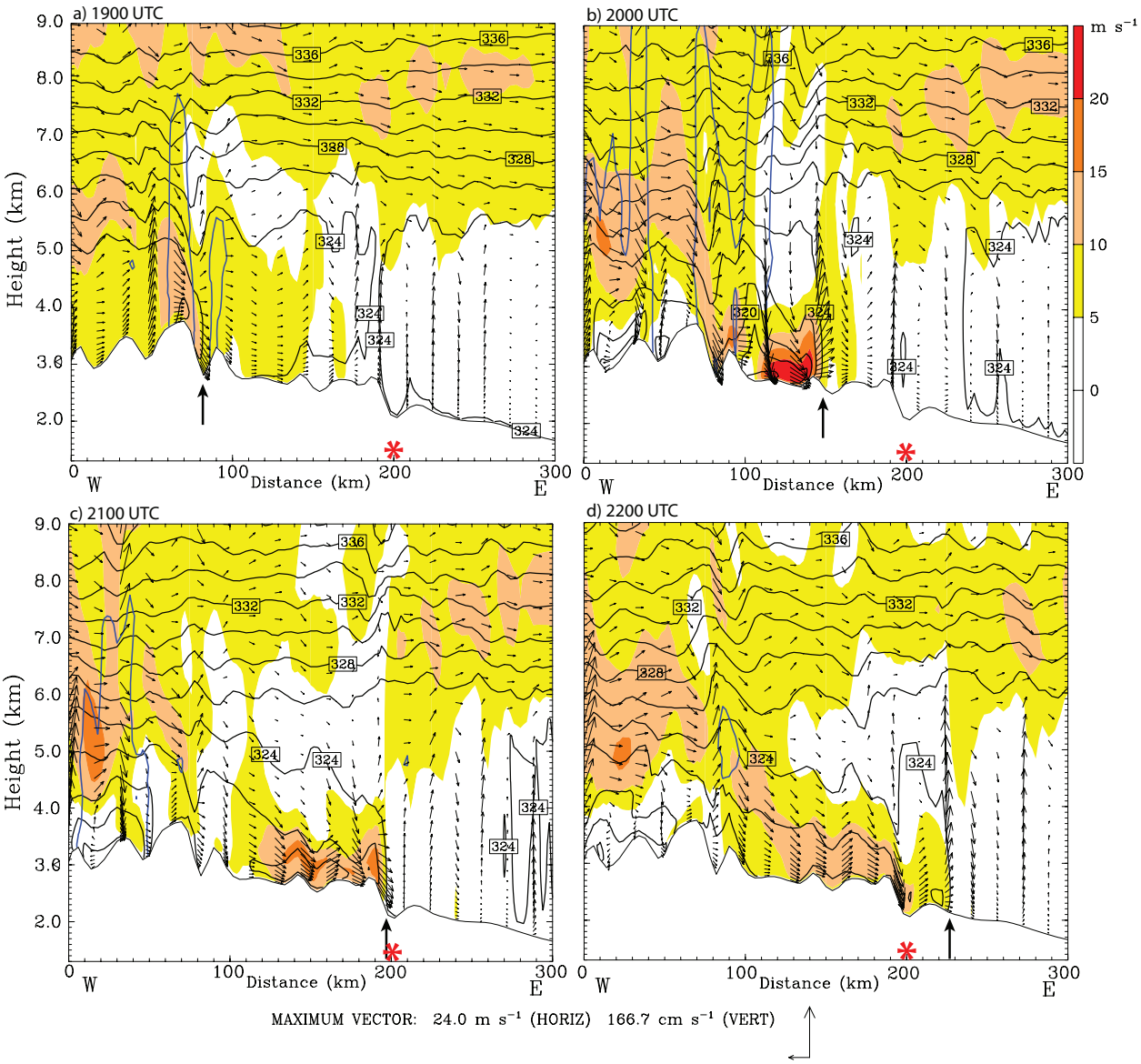

FIG. 19. East-west cross section (see Fig. 18 for location) of simulated winds (vectors, with magnitude in m s^{-1} in color) and potential temperature (K) from (a-d) 1900 to 2200 UTC, 26 June 2012. Location of precipitation is indicated by 20-dBZ simulated reflectivity contours (blue). Leading edge of gust front is marked by arrow and longitude of fire by asterisk.